Catalysis Science and Technology

ROYAL SOCIETY OF CHEMISTRY

ARTICLE

Insights into mechanism and selectivity in ruthenium(II)-catalysed *ortho*-arylation reactions directed by Lewis basic groups

Jamie McIntyre,[a] Irene Mayoral-Soler,[a,b] Pedro Salvador,*[b] Albert Poater,*[b] and David J. Nelson*[a]

We report a detailed study of the selectivity of ruthenium-catalysed C-H arylation reactions directed by Lewis basic heterocycles. A reactivity scale for directing power in these reactions, based on the results of intermolecular competition experiments, is reported for the first time. Our work is supported by detailed density functional theory calculations that reveal the underlying mechanism of this reaction, which requires the dissociation of a *p*-cymene ligand before oxidative addition becomes competent. The calculated energetic span of the catalytic cycles for each substrate is broadly in agreement with our experimental observations. This work advances our understanding of mechanism and selectivity in these reactions, and provides a basis for future catalyst design efforts.

Introduction

The development of robust, scalable, and economical C-H activation reactions still represents a major challenge in the field of organometallic chemistry, catalysis, and organic synthesis.[1] Site-selectivity is a key hurdle in these reactions due to the preponderance of C-H bonds in organic molecules. Progress towards understanding site selectivity in C-H activation reactions has been made, but most examples consider very specific transformations and require considerable time, resources and/or computational horsepower.[2-5] One approach to enforce site selectivity is to use a Lewis basic directing group. The site of functionalisation is typically *ortho*- to the directing group, although examples have been reported that are *meta*-selective and proceed *via* mechanisms that possibly involve radical intermediates.[6-11]

This strategy has been effective with rhodium, iridium, palladium, nickel, and ruthenium catalysts.[12-15] For example, Ruthenium-catalysed reactions[16] make widespread use of this approach with catalysts such as $[RuCl_2(\textit{p}\text{-cymene})(PPh_3)]$[17] and $[Ru(O_2CR)_2(\text{p-cymene})]$.[18] Reactions catalysed by the latter type proceed *via* relatively facile concerted deprotonation/ruthenation (known as concerted metalation/deprotonation (CMD) or ambiphilic metal-ligand activation (AMLA)),[19] which occurs at an appreciable rate even at room temperature.[20, 21] This type of ruthenium catalyst can also mediate C-H arylation by the combination of benzoic acids with aryl halides.[22, 23] Experimental evidence suggests that this process occurs in an

intermolecular fashion. Rate-limiting oxidative addition is proposed to lead to the product in arylation reactions where aryl halides are used, while other examples of C-H functionalisation reactions use boronic acid coupling partners.[24] Understanding oxidation state changes during catalytic cycles is very important.[25] Several researchers have carried out computational studies of reactions catalysed by complexes of the form $[RuX_2(\eta^6\text{-arene})]$,[26] but there has not yet been a study of the oxidative addition of aryl halides to plausible intermediates on this type of catalytic cycle. Larrosa studied C-H activation by $[Ru(NC^tBu)_4(OPiv)]^+$ complexes, while Prabhu,[27] and McMullin and Frost,[28] have calculated free energy profiles for C-H activation by $[Ru(OAc)_2(\eta^6\text{-arene})]$ species.

To date, we have only a semi-quantitative understanding of how strongly different groups direct the metal centre and influence reactivity. An example is the qualitative ranking for palladium-catalysed arene acetoxylation,[29] where a 8-aminoquinoline-derived amide was shown to be a stronger directing group than common *N*-heterocycles.[30] This issue is important because functionalised substrates such as intermediates *en route* to pharmaceuticals, agrochemicals, or materials may contain a variety of (potentially directing) functional groups. A detailed understanding of selectivity will allow reaction planning and the development of protocols or catalysts to change this selectivity. Moreover, the choice of directing group can affect not only the energetic barriers to reaction but also the mechanism.[31]

Only a few reactions that aim to establish the order of reactivity in ruthenium catalysis have been reported.[32-34] Competition oxidation experiments carried out with arene substrates established that the directing power decreases as amide > carbamate > ester. Subsequently it was shown that the directing power decreased as amide > ketone >> aldehyde. In an oxidative C-H vinylation reaction, the directing group power decreased as ketone > carboxylic acid > oxazolidinone > ester >

a. *WestCHEM Department of Pure and Applied Chemistry, University of Strathclyde, 295 Cathedral Street, Glasgow, G1 1XL, UK. david.nelson@strath.ac.uk*

b. *Institut de Química Computacional i Catàlisi and Departament de Química, Universitat de Girona, Campus Montilivi, 17003 Girona, Catalonia, Spain. albert.poater@udg.edu; pedro.salvador@udg.edu*

aldehyde.[28] These interesting examples are semi-quantitative at best, and consider reactions that use strong oxidants.

This work describes our efforts towards building a quantitative understanding of directing group ability of different Lewis basic groups, and the underlying reaction mechanisms that lead to this selectivity (Figure 1).
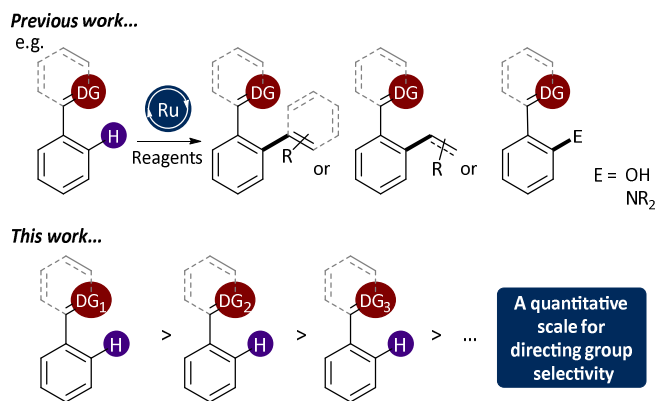

Figure 1. Ruthenium-catalysed C-H activation and selectivity.

Results and discussion

Constructing a reactivity scale for directing group power

Ackermann's conditions for arylation[18] were selected (see Scheme 1) for this study, because i) they use a well-defined catalyst (**1**), ii) they were shown to be applicable to multiple substrates and iii) they concern the construction of important structural motifs. The use of 0.5 equivalents of chlorobenzene ensured selectivity for the mono-arylated product. The reaction proceeded with pyridines, pyrazoles, oxazolines, imidazoles, and imines. A series of exploratory reactions established that other – presumably weaker – directing groups such as aldehydes, amides, and carbamates are unfortunately unreactive under these reaction conditions. The attempted reactions with these substrates led only to the recovery of the starting material, as determined by GC-FID analysis.
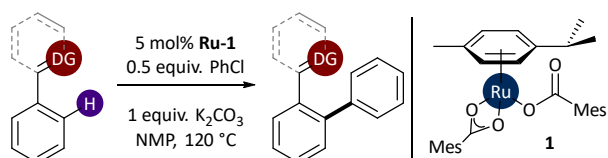
Scheme 1. Conditions selected for this study; NMP = *N*-methylpyrrolidone.

Competition reactions were conducted, each with two substrates and a limiting amount of chlorobenzene; 2-phenylpyridine (**2**), 1-phenylpyrazole (**3**), 2-phenyloxazoline (**4**), 1-methyl-2-phenylimidazole (**5**), and *N*-(1-phenylethylidene) aniline (**6**) were used. Approximately equimolar quantities of each of the two substrates were employed, with one 5 mol% charge of catalyst (**1**) and 0.5 equiv. of chlorobenzene. The GC-FID apparatus was calibrated for all substrates and products (2-([1,1'-biphenyl]-2-yl)pyridine (**7**); 1-([1,1'-biphenyl]-2-yl) pyrazole (**8**); 2-([1,1'-biphenyl]-2-yl)oxazoline (**9**); 2-([1,1'-biphenyl]-2-yl)-1-methyl-imidazole (**10**); and 1-([1,1'-biphenyl]-

2-yl)-*N*-phenylethan-1-imine (**11**)) using samples of the authentic compounds. Compounds **5**, **6**, and **11** (*via* **12**) were prepared according to Scheme 2. Competition reactions were conducted in duplicate, and the concentrations of each starting material and product were quantified by GC-FID analysis, by integration of the analyte peaks *versus* an internal standard (tetradecane).
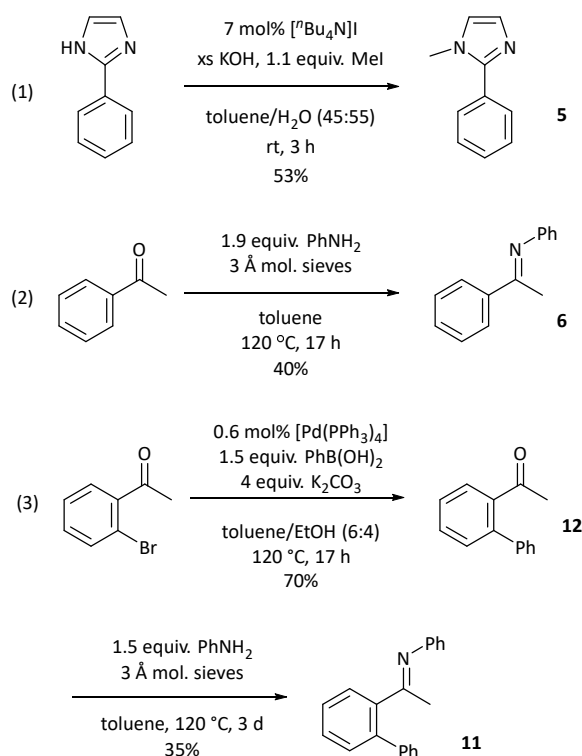
Scheme 2: Synthesis of substrates **5** and **6**, and product **11**.

To construct the directing group power scale, competition, the constant κ – which quantifies the relative rates of two competing processes with rates k_1 and k_2 (eq. 1) – was employed.[35-37]

$$\log_{10}(\kappa) = \log_{10}(k_1) - \log_{10}(k_2) = \log_{10}(k_1/k_2) \qquad (1)$$

A series of reactions were conducted, a number of values of κ were determined and linear regression was used to calculate a set of k_n values, which represent the relative rates of reaction of the different substrates. Mayr and Knochel have previously used this avenue to quantify the relative reactivity of different organozinc species in palladium-catalysed cross-coupling reactions,[36] and in magnesium/halide exchange reactions.[37] If each reaction produces only one product, quantification of the concentrations of product (P^1, P^2) and starting material (S^1, S^2) for each reaction readily delivers κ (eq. 2).

$$\kappa = \log_{10}(1 + [P^1]/[S^1]) / \log_{10}(1 + [P^2]/[S^2]) \qquad (2)$$

κ is independent of time, which was confirmed by repeating some experiments over a shorter time period. Using linear regression, values of k_{rel} were calculated for all five substrates

from the series of values for κ. Pyridine was arbitrarily assigned k_{rel} = 1. This allowed the first quantitative scale for directing group power to be constructed (Figure 2). A plot of experimental competition constants κ_{exp} versus κ_{calc} (calculated using k_{rel} from linear regression) shows that our approach is meaningful (Figure 3). The range of reactivity is surprisingly narrow, with k_{rel} = 0.03 − 1. Amongst the *N*- heterocycle directing groups the range of reactivity (k_{rel}) is only 0.17 − 1. However, our tests with other, weaker directing groups show that it should be possible to achieve the arylation of substrates **2**-**6** in the presence of weaker Lewis bases such as aldehydes and ketones.
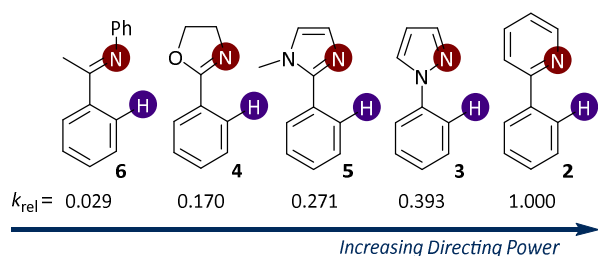

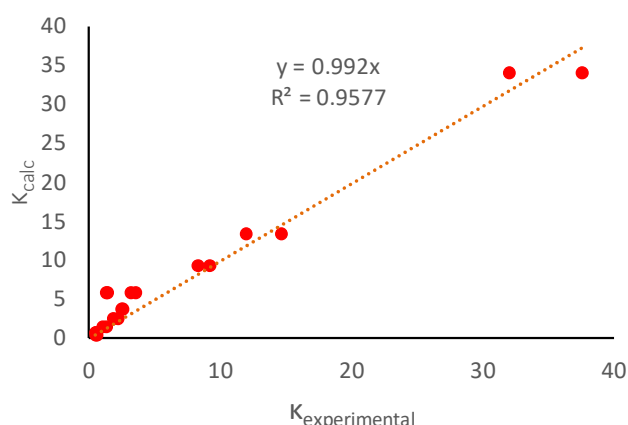**Figure 2**. A directing group power scale.

Figure 3. Plot of experimental *versus* calculated values of κ.

Various scales for Lewis acidity and Lewis basicity have been developed;[38] however, attempts to link these to the selectivity observed here were unsuccessful. Data for lithium, sodium, and potassium ion affinity/basicity are available, but only for pyridine, pyrazole, and 1-methylimidazole. The available data suggest that basicity decreases in the order 1-methylimidazole > pyridine > pyrazole, which is not the same order of reactivity that is observed in ruthenium(II)-catalysed C–H arylation reactions. This might be a consequence of the rather softer nature of Ru^{II} *versus* Li$^+$, Na$^+$, and K$^+$, or the effect of having other ligands around the metal centre.

Insights into the reaction mechanism

As noted in the introduction, some stages of the reaction mechanism with complexes of this type have been well explored.[20, 21] However, the latter half of the catalytic cycle – i.e. oxidative addition of the aryl halide – is still poorly understood.

The active catalyst is known to be a [Ru(O$_2$CR)$_2$(*p*-cymene)] species (**I**), where *R*=Me, Mes or Ad, as studied by Jutand and Dixneuf, and by Ackermann[18, 20, 21] (Scheme 3). The mechanism proceeds according to the following steps. An acetate ligand is displaced by an incoming substrate molecule with a Lewis basic directing group (**II**). Then, an intermolecular C–H activation/ruthenation takes place to yield complex **III**.
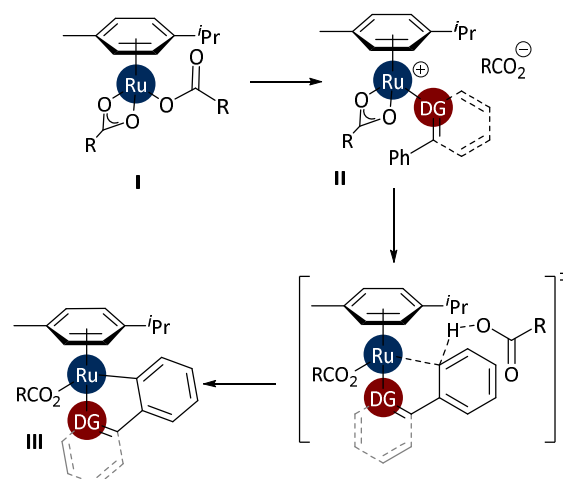
Scheme 3. Experimentally-established mechanism for metalation at the C–H bond *ortho*- to a Lewis basic directing group by complex **I**.

Unfortunately, there are precious few insights into how oxidative addition takes place to **III** to complete the cycle and deliver the desired product. Ackermann has conducted Hammett studies on a model reaction between and azobenzene and differently substituted aryl bromides, catalysed by [Ru(O$_2$CMes)$_2$(*p*-cymene)] (generated *in situ*), which showed zero order behaviour to at least 50% conversion;[39] this yielded ρ = -0.2, suggesting that *electron-rich* aryl bromides react most quickly, and prompting the authors to propose rate-limiting reductive elimination. In contrast, other studies have revealed two-phase Hammett plots with ρ ≈ 0.4 where σ$_p$ < 0 and ρ < 0 where σ$_p$ > 0.[40, 41]

In attempts to probe the latter step experimentally, we prepared known complexes[42] of the same structure as **III** and exposed these to aryl halides in toluene solution, and monitored reactions by ^{1}H NMR or UV/visible spectroscopy. Unfortunately, oxidative addition did not occur. Jutand noted the need for additives such as a base to enable complexes such as **III** to undergo oxidative addition.[20] Recent experimental evidence from Larrosa[43] and Frost[11] strongly suggests that the *p*-cymene ligand must dissociate from the complex in order for reactions to occur; Larrosa's work was supported with preliminary DFT calculations.

We then embarked on a computational study of the reaction mechanism to gain new insight into how this oxidative addition step proceeds, and to rationalise and further understand the observed order of selectivity. This study was performed using density functional theory (DFT) including implicit NMP (see Computational Details). For our computational study, the acetate complex [Ru(OAc)$_2$(*p*-cymene)] (**A**) was considered (R = Me). Our two main aims were to: (i) establish whether the

This journal is © The Royal Society of Chemistry 2018

Catal. Sci. Technol., 2018, **00**, 1-3 | **3**

reaction mechanism suggested in the literature is feasible under the reaction conditions utilised here; and (ii) to identify whether this reaction mechanism can explain observed trends in reaction selectivity that we have established here experimentally.

In order to assess the relative rates of different reactions computationally, the concept of 'energetic span' has been employed.[44] This does not consider one specific fundamental step to be rate-determining, but instead looks at the difference between the highest and lowest points of the free energy surface. The overall energetic span (δE) of the catalytic cycle depends on the order in which the turnover-frequency determining transition state (TDTS) and turnover-frequency determining intermediate (TDI) occur. If the TDTS occurs first, δE is calculated according to equation (3), otherwise equation (4) applies.

$$\delta E = T_{TDTS} - I_{TDI} + \Delta G_r \qquad \text{(TDTS occurs first)} \qquad (3)$$
$$\delta E = T_{TDTS} - I_{TDI} \qquad \text{(TDI occurs first)} \qquad (4)$$

Initially, a free energy profile was calculated for the reaction of **A** with substrate **2** to form **D**, followed by oxidative addition of PhCl and formation of the product (**7**) (Figure 4). For this reaction mechanism, the TDTS is **TS-E-F**, the TDI is **H** and ΔG_r for the reaction is 27.0 kcal mol^{-1}. The energetic span calculated using equation (3) is found to be 59.8 kcal mol^{-1}. Note that the oxidative addition transition state (**TS-E-F**) is very high in energy (64.1 kcal mol^{-1}), so this mechanism is not likely to be feasible even under the rather forcing reaction conditions that are used experimentally (120 °C). A reaction *via* cationic intermediates in which an acetate ligand has been dissociated can be ruled out based on a range of evidence: cationic species [Ru(OAc)(*p*-cymene)(2-phenylpyridine)]$^+$ is found to be 17.1 kcal/mol higher in energy with respect to **A**; the highest energy transition state with acetate dissociated is still destabilized by 1.5 kcal/mol with respect to the highest energy transition state in Figure 4; and the reaction is known to proceed on a similar timescale in toluene solvent, which has a much lower dielectric constant than NMP (2.4 and 32.6, respectively) and would therefore disfavour dissociation of a charged ligand.[45]

Further computational analysis permitted the location of an alternative oxidative addition transition state (**TS-E-F'**), in which the hapticity of the *p*-cymene ligand was decreased as oxidative addition took place; this leads to dissociation of the *p*-cymene ligand and formation of **F'**. This transition state is lower in energy by 15.8 kcal mol^{-1} as compared to the **TS-E-F**, so such a

Figure 4. Free energy surface for the arylation of 2-phenylpyridine with chlorobenzene, catalysed by [Ru(OAc)$_2$(*p*-cymene)], in a mechanism where *p*-cymene remains bound to the metal centre throughout. Energies are free energies in kcal mol^{-1} relative to complex **A**, in NMP solvent.

4 | Catal. Sci. Technol., 2018, **00**, 1-3

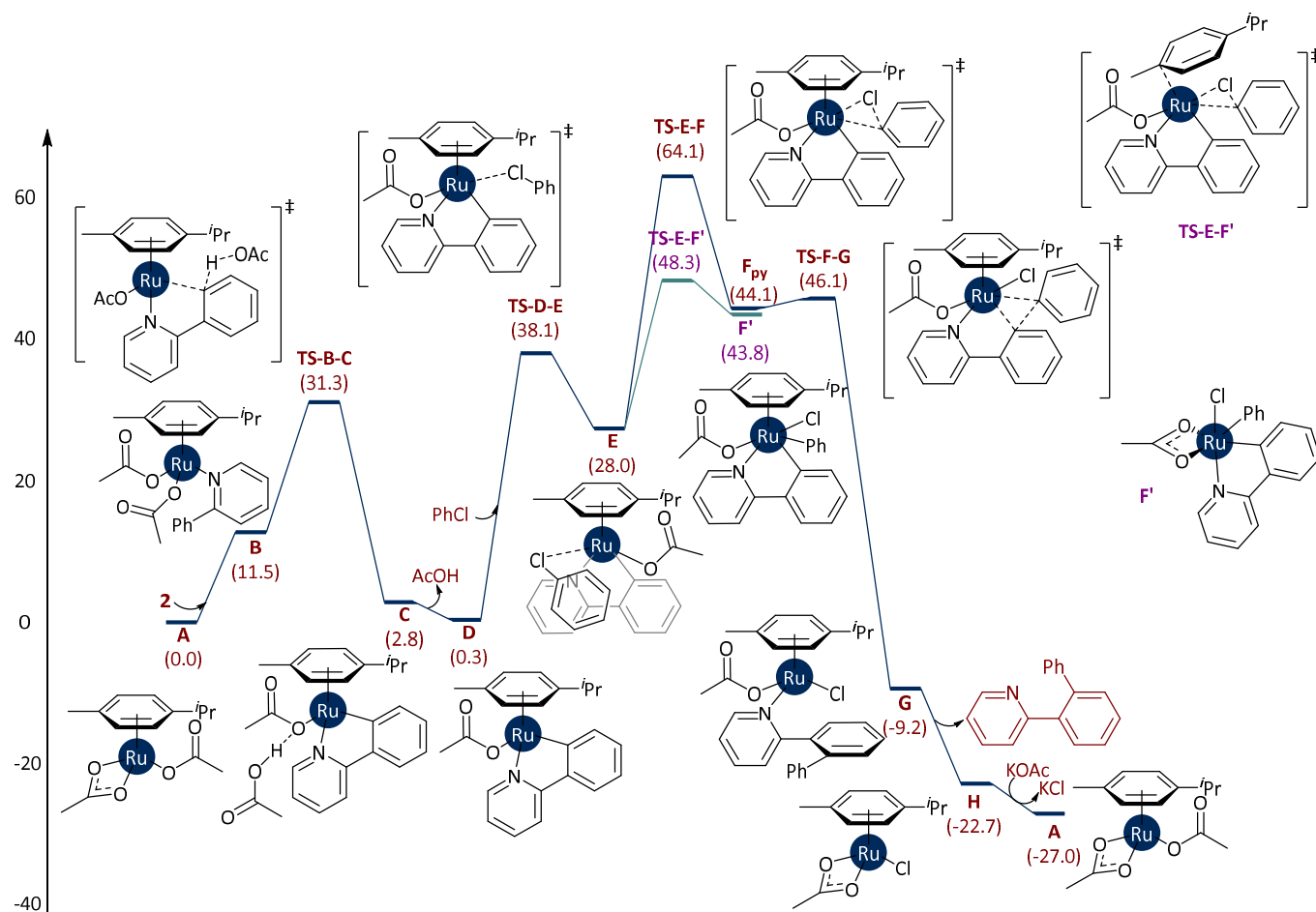This journal is © The Royal Society of Chemistry 2018

Figure 5. Free energy surface for the arylation of 2-phenylpyridine with chlorobenzene, catalysed by [Ru(OAc)₂(*p*-cymene)], in a mechanism where *p*-cymene is not bound to the metal centre. Energies are free energies in kcal mol⁻¹ relative to complex **A**, in NMP solvent.

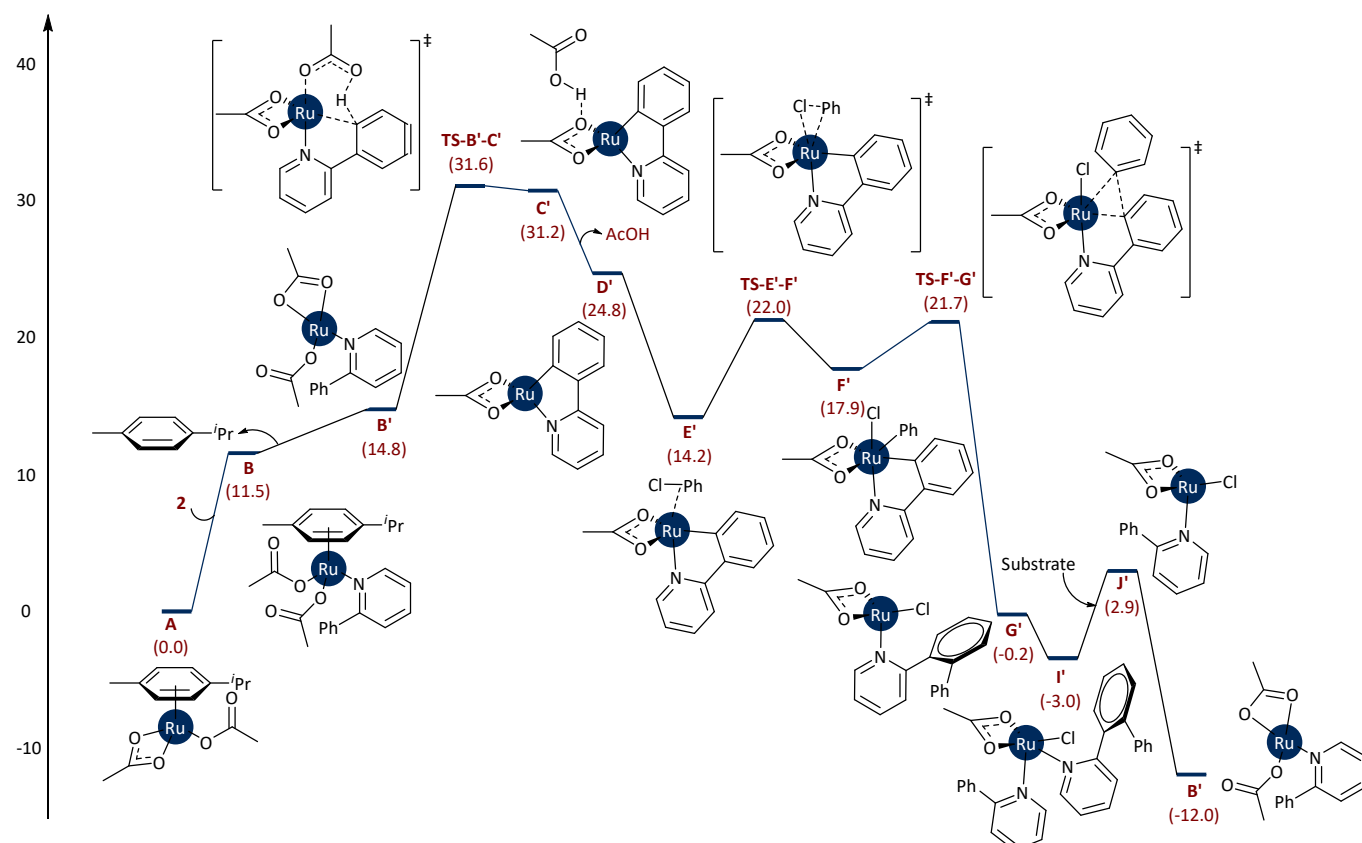ligand dissociation event would occur in preference to an oxidative addition reaction to form **F**. Based on this observation and evidences from the studies by Larrosa[43] and Frost,[11] an alternative free energy profile was calculated in which no *p*-cymene ligand was present (Figure 5). Again, C-H activation is achieved by a tandem deprotonation/metalation mechanism, but this time in an intramolecular fashion. Oxidative addition and reductive elimination are much more facile, and the overall energetic span of the cycle is much lower. The TDTS is **TS-B'-C'** (ΔG_{rel} = 31.6 kcal mol⁻¹) and the TDI is **I'** (ΔG_{rel} = -3.0 kcal mol⁻¹), with an overall ΔG_r of -26.8 kcal mol⁻¹. The energetic span calculated using equation (4) is just 7.8 kcal mol⁻¹. Finally, the coordinating capability of NMP was also tested, but **B'** bearing NMP as a ligand was found to be 14.1 kcal/mol higher in energy, so NMP-ligated species are unlikely to be involved.

The main conclusion that emerges from these results is that the *p*-cymene ligand must be removed during the first turnover of the cycle, during oxidative addition (Figure 4). Once this occurs, subsequent catalytic cycles proceed *via* a sequence of intermediates which have no *p*-cymene ligand bound. The energetic span for this cycle is much smaller, hence it will turn over more quickly. The initial turnover will require much higher temperatures than subsequent turnovers in order to achieve *p*-cymene dissociation. Complexes without *p*-cymene ligands, or that bear more labile η⁶-arene ligands, may therefore yield more reactive catalysts for future generations of C-H activation reactions. This pathway is dependent on the presence of carboxylate ligands bound to ruthenium. Arene-free catalysts for C-H functionalisation are widely known, such as recent examples from the groups of Larrosa[43] and Frost;[11] Štefane profiled the release of *p*-cymene during a prototypical C-H arylation reaction.[40] The present study demonstrates that not only are arene-free complexes *more* reactive than arene-containing catalysts, but that arene-containing catalysts are *ineffective* for C-H arylation reactions. This is important given the preponderance of arene-containing ruthenium complexes in the C-H functionalisation literature,[15] despite the demonstrated competence of alternative precursors such as [RuH₂(CO)(PPh₃)₃],[46] [RuH(COD)₂][BF₄],[47] and even RuCl₃.nH₂O[48-51] in C-H arylation reactions; in addition, arene-free ruthenium carboxylate complexes and even ruthenium alkylidenes have been deployed in C-H alkylation reactions.[52, 53]

Analysis of oxidation states

Additional insight into the electronic structures of the intermediate species in Figure 5 was obtained using the effective oxidation states (EOS) analysis.[54] This approach has recently been used to probe the electronic structure of ruthenium complexes that possess potentially non-innocent ligands.[55] In particular, we wished to establish the formal oxidation state of the ruthenium centre as it progresses through the catalytic cycle. Table 1 presents three important pieces of data for each structure, namely: the formal oxidation state of ruthenium in this structure; the partial atomic charge of the ruthenium atom; and the R index derived from EOS analysis. The latter indicates how closely the actual electron distribution within the molecule agrees with the formal ionic picture of oxidation states. The lowest possible value of R is 50%, which indicates that two different assignments are equally probable.

The values obtained show that all structures, with the exception of **TS-E'-F'** and **F'** are best described as ruthenium(II)

Table 1. Analysis of oxidation state, R-index, and partial charge on ruthenium (Q_{Ru}) for structures in Figure 5.

Structure	Oxidation State	R	Q_{Ru}
A	Ru(II)	91%	1.50
B	Ru(II)	95%	1.54
B'	Ru(II)	93%	1.64
TS-B'-C'	Ru(II)	100%	1.59
C'	Ru(II)	64%	1.26
D'	Ru(II)	65%	1.27
E'	Ru(II)	64%	1.41
TS-E'-F'	Ru(IV)	50%	1.51
F'	Ru(IV)	51%	1.45
TS-F'-G'	Ru(II)	67%	1.48
G'	Ru(II)	97%	1.45
I'	Ru(II)	93%	1.56
J'	Ru(II)	89%	1.52

complexes. Structures **C**, **D**, and **E** have lower R indices, perhaps as a consequence of the bidentate coordination of the phenylpyridine substrate, which can be redox non-innocent. Species **TS-E'-F'** and **F'**, associated with the oxidative addition step, can be considered to have ruthenium(IV) character but the low R index (close to 50%) suggests an almost equivalent contribution of ruthenium(II). Contrary to what is sometimes believed, the value of the partial charge on ruthenium is completely unrelated to its formal oxidation state and character.

Predicting selectivity in arylation reactions

With a free energy profile for the arylation of **2** established, studies were extended to evaluate selectivity in the competition reactions discussed previously. Free energy profiles for all five substrates (**2**-**6**) were calculated, and the energies of the intermediates and transition states are gathered in Table 2. Full potential energy profiles for all substrates can be found in the Supporting Information.

In all cases, **TS-B'-C'** is the TDTS, whereas **I'** is typically the TDI, except for substrate **4** (imidazole) where it corresponds to **G'**. With the exception of substrate **6** (imine) the trend in δE mirrors the trend in k_{rel} from competition experiments, namely the energetic spans increase in the order **2** < **3** < **5** < **4**, reflecting a decrease in the rate of reaction. Notably, the energies of any of the specific barriers or intermediates do not show a well-defined trend, so the energetic span of the overall cycle needs to be considered in order to reproduce the experimental trends.

Conclusions

We have carried out a detailed and quantitative study of mechanism and selectivity in C-H arylation reactions catalysed by ruthenium carboxylate complexes. Experimental studies have produced a quantitative ranking of five commonly-used directing groups based on nitrogen-containing functional groups, revealing a rather narrow window of reactivity (k_{rel} = 0.03 − 1). DFT calculations have provided new insight into the identity of the active catalyst in these systems and how this active species is generated *in situ*. A mechanism involving a *p*-cymene-ligated complex was elucidated but the oxidative addition to chlorobenzene has a prohibitively high barrier. The location of an alternative low-energy TS in which the *p*-cymene ligand dissociates during oxidative addition paved the way for a more plausible, alternative pathway in which the active catalyst does not bear an arene ligand.

Conflicts of interest

There are no conflicts to declare.

Acknowledgements

Computational Details

All calculations were carried out using Gaussian09 (Rev. E.01).[56] The SDD pseudopotential/ECP was used for ruthenium in all calculations. Structures were optimised at the BP86-D3/SVP level of theory, and energies were refined using M06/CC-pVTZ.

6 | Catal. Sci. Technol., 2018, **00**, 1-3

This journal is © The Royal Society of Chemistry 2018

Table 2. Energies of key intermediates and transition states in the ruthenium-catalysed C-H arylation reactions of **2 – 6** using PhCl.[a]

Substrate	2	3	4	5	6
Directing Group	*Pyridine*	*Pyrazole*	*Oxazoline*	*Imidazole*	*Imine*
Pre-catalyst (A)	0.0	0.0	0.0	0.0	0.0
Substrate coordinated (B)	11.5	7.9	5.4	3.1	9.6
Without *p*-cymene ligand (B')	14.8	18.4	18.5	15.7	12.6
C-H activation (TS-B'-C')	31.6	36.6	38.9	34.3	32.9
Metalated intermediate.AcOH (C')	31.2	31.0	33.5	30.7	29.3
Metalated intermediate (D')	24.8	25.4	27.9	26.1	23.1
Chlorobenzene coordinated (E')	14.2	15.7	17.3	15.2	12.6
Oxidative addition (TS-E'-F')	22.0	25.0	26.2	23.1	21.0
Ru(IV) intermediate (F')	17.9	17.6	13.4	9.3	8.8
Reductive elimination (TS-F'-G')	21.7	26.1	25.4	22.5	21.9
Product coordinated (G')	-0.2	0.5	-1.4	-4.1	1.7
Product and substrate coordinated (I')	-3.0	-1.0	1.5	-7.9	0.2
Product decoordination (J')	2.9	5.9	7.5	1.9	1.4
Substrate coordinated (B')	-12.0	-9.4	-8.0	-13.5	-14.7
Turnover-determining Transition State (TDTS)	**TS-B'-C'**	**TS-B'-C'**	**TS-B'-C'**	**TS-B'-C'**	**TS-B'-C'**
Turnover-determining Intermediate (TDI)	**I'**	**I'**	**G'**	**I'**	**I'**
Free Energy of Reaction (ΔG_r)	-26.8	-27.8	-26.5	-29.2	-27.3
Energetic Span (δE)	7.8	9.8	13.8	13.0	5.4

[a] Energies are free energies in kcal mol^{-1} in NMP solvent.

NMP solvent was modelled using a polarisable continuum model (PCM). The nature of stationary points on the free energy surface was confirmed using frequency calculations.

Experimental

General. NMR spectra were acquired at 300 K using a Bruker AV3-400 spectrometer fitted with a liquid nitrogen cryoprobe. ^{1}H NMR spectra are referenced to the residual solvent signal. ^{13}C{^{1}H} NMR spectra are referenced to solvent signals.

GC-MS data were acquired on an Agilent Technologies 7890A GC system fitted with a Restek Rxi-5Sil column (30 m, 0.25 mm ID, 0.25 µm) and coupled to an Agilent mass spectrometer using either chemical ionisation (methane) or electron impact ionisation. Helium was used as the carrier gas (1 mL min^{-1}). In all cases, an inlet temperature of 320 °C and the following oven temperature gradient were used: 4 min at 40 °C; ramp to 320 °C at 20 °C min^{-1}; hold for 10 min (total run time of 28 min). GC-FID data were acquired on an Agilent Technologies 7890A GC system fitted with a Restek Rxi-5Sil column (30 m, 0.32 mm ID, 0.25 µm). Helium was used as the carrier gas (2 mL min^{-1}). Hydrogen (30 mL min^{-1}) and compressed air (400 mL min^{-1}) were used for the FID. An inlet temperature of 320 °C was used, as well as the following oven temperature gradient: 5 min at 40 °C; ramp to 320 °C at 20 °C min^{-1}; hold for 5 min (total run time 24 min).

Column chromatography was performed using silica gel (Zeochem Zeoprep 60 HYD, 40 – 63 µm). Thin layer chromatography was performed on pre-coated aluminium-backed silica gel plates (Merck silica gel 60, F254, 0.2 mm). Melting points were acquired using a Griffin EN61010-1.

[Ru(O$_2$CMes)$_2$(*p*-cymene)] was prepared according to literature procedures.[18] 2-phenylpyridine (**2**), 1-phenylpyrazole (**3**), and phenyloxazoline (**4**) were obtained from commercial sources and used as supplied. Arylated products **7-10** were prepared according to literature methods.[18] Complexes of the general form **III** were prepared using literature methods.[42, 57]

***N*-methyl-2-phenylimidazole (5).** A round-bottom flask was charged with 2-phenylimidazole (5.00 g, 35 mmol), tetra-*n*-butylammonium iodide (0.92 g, 2.5 mmol), toluene (150 mL), and 33% *w/w* aqueous potassium hydroxide solution (190 mL). The reaction was stirred using an overhead stirrer. Iodomethane (2.4 mL, 38.5 mmol) was added and the reaction was stirred at room temperature for 3 h. Distilled water (200 mL) and toluene (100 mL) were added. The layers were separated, and the organic layer was washed with saturated aqueous sodium thiosulfate solution, dried on magnesium sulfate, and evaporated under reduced pressure to yield an orange oil which crystallised on standing. Yield: 2.9 g, 53%. **^{1}H NMR** (400 MHz, CDCl$_3$) δ_H 7.60 – 7.57 (m, 2H, Ar C-H), 7.43 – 7.33 (m, 3H, Ar C-H), 7.08 (d, 1H, C-H, $^3J_{HH}$ = 1.2 Hz), 6.91 (d, 1H, C-H, $^3J_{HH}$ = 1.2 Hz), 3.67 (s, 3H, N-CH$_3$). **^{13}C{^{1}H} NMR** (101 MHz, CDCl$_3$) δ_C 147.3, 130.2, 128.1, 128.0, 128.0, 127.9, 121.9, 33.9. **m/z** (GC-MS, CI): 159.1 [M+H]+, 187.1, 199.1. Analytical data are consistent with the literature.[58]

***N*-(1-phenylethylidene)aniline (6).** A round-bottom flask was charged with toluene (10 mL), freshly-dried 3 Å molecular sieves, acetophenone (2 mL, 17.1 mmol), and aniline (3 mL, 32.9 mmol). The reaction was stirred at 120 °C for 17 h and filtered

to remove molecular sieves. The solvent was removed under reduced pressure and the product was purified by Kugelrohr distillation (150 °C, 0.6 mbar) to yield a pale solid. Yield: 1.4 g, 40%. **M.P.** 38 – 41 °C. **¹H NMR** (400 MHz, CDCl₃) δ_H 8.05 – 8.02 (m, 2H, Ar C-H), 7.52 – 7.48 (m, 3H, Ar C-H), 7.40 (t, 2H, Ar C-H, J = 7.6 Hz), 7.14 (tt, 1H, Ar C-H, J = 7.5, 1.2 Hz), 6.87 – 6.85 (m, 2H, Ar C-H), 2.28 (s, 3H, C-CH₃). **¹³C{¹H} NMR** (101 MHz, CDCl₃) δ_C 165.0, 151.3, 139.1, 130.0, 128.5, 127.9, 126.7, 122.7, 118.9, 16.9. **m/z** (GC-MS, CI): 196.1 [M+H]+, 224.1, 236.1. Analytical data are consistent with the literature.[59]

2'-phenyl-acetophenone (**12**). A flame-dried round-bottom flask was charged with [Pd(PPh₃)₄] (49 mg, 0.042 mmol), toluene (70 mL) and ethanol (46 mL) forming a yellow solution. Phenylboronic acid (1.3 g, 10.5 mmol), potassium carbonate (4 g, 28 mmol) and 2'-bromoacetophenone (0.95 mL, 7 mmol) were added and the reaction was stirred at 120 °C for 17 h. The solvent volume was decreased under reduced pressure, and the solution was filtered through celite. The product was purified by Kugelrohr distillation (170 °C, 14 mbar) to yield a colourless oil. Yield: 0.96 g, 70%. **¹H NMR** (400 MHz, CDCl₃) δ_H 7.58 – 7.51 (m, 2H, Ar C-H), 7.45 – 7.36 (m, 7H, Ar C-H), 2.04 (s, 3H, C(O)CH₃). **¹³C{¹H} NMR** (101 MHz, CDCl₃) δ_C 204.4, 140.4, 140.3, 140.1, 130.3, 129.8, 128.4, 128.2, 127.4 (2 carbons), 127.0, 30.0. **m/z** (GC-MS, CI): 197.1 [M+H]+, 179.0. Analytical data are consistent with the literature.[60]

N-(1-2'phenyl-phenylethylidene)aniline (**11**). A round-bottom flask was charged with 2'-phenyl-acetophenone (0.5 g, 2.5 mmol), aniline (360 μL, 3.75 mmol), toluene (2 mL) and freshly-dried 3 Å molecular sieves. The reaction was stirred at 120 °C for 3 d, and filtered to remove the molecular sieves. The solvent was removed under reduced pressure to yield a red-black oil which was purified by column chromatography on silica gel (10 % Et₂O/hexane) to give a yellow oil. Recrystallisation from hexane gave the product as a yellow solid as 1:0.18 mixture of E and Z isomers. Yield: 240 mg, 35%. Major (E): **¹H NMR** (400 MHz, CDCl₃) δ_H 7.64 (d, 1H, Ar C-H, J = 7 Hz), 7.56 – 7.52 (m, 2H, Ar C-H), 7.51 – 7.45 (m, 5H, Ar C-H), , 7.38 – 7.33 (m, 3H, Ar C-H), 7.09 (tt, 1H, Ar C-H, J = 7.4 Hz, 1.2 Hz), 6.80 – 6.77 (m, 2H, Ar C-H), 2.47, 1.70 (s, 3H, CH₃). **¹³C{¹H} NMR** (101 MHz, CDCl₃) δ_C 170.9, 150.7, 141.3, 140.9, 139.4, 129.6, 128.6, 128.48, 128.47, 128.0, 127.7, 127.0, 126.9, 122.9, 118.7, 20.9. **m/z** (GC-MS, CI): 272.1 [M+H]+, 256.0, 179.0. **Anal.** Calc'd for C₂₀H₁₇N: C, 88.52; H, 6.31; N, 5.16. Found: C, 88.27; H, 6.33; N, 5.17. Analytical data are consistent with the literature.[61]

Notes and references

§ See the Supporting Information for: characterisation data for **5**, **6**, **11**, and **12**; calibration data for **2-11** versus tetradecane for GC-FID quantification; coordinates and energies for all intermediates and transition states modelled using DFT calculations.

1. J. A. Labinger and J. E. Bercaw, *Nature*, 2002, **417**, 507-514.
2. E. N. Bess, D. M. Guptill, H. M. L. Davies and M. S. Sigman, *Chem. Sci.*, 2015, **6**, 3057-3062.
3. K. Liao, S. Negretti, D. G. Musaev, J. Bacsa and H. M. L. Davies, *Nature*, 2016, **533**, 230-234.
4. H. Choi, M. Min, Q. Peng, D. Kang, R. S. Paton and S. Hong, *Chem. Sci.*, 2016, **7**, 3900-3909.
5. K. J. T. Carr, D. L. Davies, S. A. Macgregor, K. Singh and B. Villa-Marcos, *Chem. Sci.*, 2014, **5**, 2340-2346.
6. O. Saidi, J. Marafie, A. E. W. Ledger, P. M. Liu, M. F. Mahon, G. Kociok-Köhn, M. K. Whittlesey and C. G. Frost, *J. Am. Chem. Soc.*, 2011, **133**, 19298-19301.
7. A. J. Paterson, S. St John-Campbell, M. F. Mahon, N. J. Press and C. G. Frost, *Chem. Commun.*, 2015, **51**, 12807-12810.
8. N. Hofmann and L. Ackermann, *J. Am. Chem. Soc.*, 2013, **135**, 5877-5884.
9. Q. Yu, L. a. Hu, Y. Wang, S. Zheng and J. Huang, *Angew. Chem. Int. Ed.*, 2015, **54**, 15284-15288.
10. C. J. Teskey, A. Y. W. Lui and M. F. Greaney, *Angew. Chem. Int. Ed.*, 2015, **54**, 11677-11680.
11. P. Marcé, A. J. Paterson, M. F. Mahon and C. G. Frost, *Catal. Sci. Technol.*, 2016, **6**, 7068-7076.
12. T. W. Lyons and M. S. Sanford, *Chem. Rev.*, 2010, **110**, 1147-1169.
13. D. A. Colby, R. G. Bergman and J. A. Ellman, *Chem. Rev.*, 2010, **110**, 624-655.
14. G. Rouquet and N. Chatani, *Angew. Chem. Int. Ed.*, 2013, **52**, 11726-11743.
15. P. B. Arockiam, C. Bruneau and P. H. Dixneuf, *Chem. Rev.*, 2012, **112**, 5879-5918.
16. P. Nareddy, F. Jordan and M. Szostak, *ACS Catal.*, 2017, **7**, 5721-5745.
17. S. Oi, H. Sasamoto, R. Funayama and Y. Inoue, *Chem. Lett.*, 2008, **37**, 994-995.
18. L. Ackermann, R. n. Vicente, H. K. Potukuchi and V. Pirovano, *Org. Lett.*, 2010, **12**, 5032-5035.
19. L. David and F. Keith, *Chem. Lett.*, 2010, **39**, 1118-1126.
20. I. Fabre, N. von Wolff, G. Le Duc, E. Ferrer Flegeau, C. Bruneau, P. H. Dixneuf and A. Jutand, *Chem. Eur. J.*, 2013, **19**, 7595-7604.
21. E. Ferrer Flegeau, C. Bruneau, P. H. Dixneuf and A. Jutand, *J. Am. Chem. Soc.*, 2011, **133**, 10161-10170.
22. A. Biafora, T. Krause, D. Hackenberger, F. Belitz and L. J. Gooßen, *Angew. Chem. Int. Ed.*, 2016, **55**, 14752-14755.
23. R. Mei, C. Zhu and L. Ackermann, *Chem. Commun.*, 2016, **52**, 13171-13174.
24. P. Nareddy, F. Jordan, S. E. Brenner-Moyer and M. Szostak, *ACS Catal.*, 2016, **6**, 4755-4759.
25. C. C. C. Johansson Seechurn, T. Sperger, T. G. Scrase, F. Schoenebeck and T. J. Colacot, *J. Am. Chem. Soc.*, 2017, **139**, 5194-5200.
26. D. L. Davies, S. A. Macgregor and C. L. McMullin, *Chem. Rev.*, 2017, **117**, 8649-8709.
27. K. R. Bettadapur, V. Lanke and K. R. Prabhu, *Org. Lett.*, 2015, **17**, 4658-4661.
28. J. A. Leitch, P. B. Wilson, C. L. McMullin, M. F. Mahon, Y. Bhonoah, I. H. Williams and C. G. Frost, *ACS Catal.*, 2016, **6**, 5520-5529.
29. L. V. Desai, K. J. Stowers and M. S. Sanford, *J. Am. Chem. Soc.*, 2008, **130**, 13285-13293.
30. Z.-Y. Gu, C.-G. Liu, S.-Y. Wang and S.-J. Ji, *J. Org. Chem.*, 2017, **82**, 2223-2230.
31. B. E. Haines, H. Xu, P. Verma, X.-C. Wang, J.-Q. Yu and D. G. Musaev, *J. Am. Chem. Soc.*, 2015, **137**, 9022-9031.
32. F. Yang, K. Rauch, K. Kettelhoit and L. Ackermann, *Angew. Chem. Int. Ed.*, 2014, **53**, 11285-11288.
33. W. Liu and L. Ackermann, *Org. Lett.*, 2013, **15**, 3484-3486.
34. P. Nareddy, F. Jordan and M. Szostak, *Org. Lett.*, 2018, **20**, 341-344.
35. R. Huisgen, *Angew. Chem. Int. Ed. Engl.*, 1970, **9**, 751-762.
36. Z.-B. Dong, G. Manolikakes, L. Shi, P. Knochel and H. Mayr, *Chem. Eur. J.*, 2010, **16**, 248-253.

37. L. Shi, Y. Chu, P. Knochel and H. Mayr, *Org. Lett.*, 2012, **14**, 2602-2605.
38. *Lewis Basicity and Affinity Scales: Data and Measurement*, John Wiley & Sons, Ltd, 2009.
39. J. Hubrich, T. Himmler, L. Rodefeld and L. Ackermann, *ACS Catal.*, 2015, **5**, 4089-4093.
40. P. Kuzman, F. Požgan, A. Meden, J. Svete and B. Štefane, *ChemCatChem*, 2017, **9**, 3380-3387.
41. D. Zell, S. Warratz, D. Gelman, S. J. Garden and L. Ackermann, *Chem. Eur. J.*, 2016, **22**, 1248-1252.
42. B. Li, C. Darcel, T. Roisnel and P. H. Dixneuf, *J. Organomet. Chem.*, 2015, **793**, 200-209.
43. M. Simonetti, G. J. P. Perry, X. C. Cambeiro, F. Juliá-Hernández, J. N. Arokianathar and I. Larrosa, *J. Am. Chem. Soc.*, 2016, **138**, 3596-3606.
44. S. Kozuch and S. Shaik, *Acc. Chem. Res.*, 2011, **44**, 101-110.
45. J. L. M. Abboud and R. Notari, *Pure Appl. Chem.*, 1999, **71**, 645-718.
46. F. Kakiuchi, Y. Matsuura, S. Kan and N. Chatani, *J. Am. Chem. Soc.*, 2005, **127**, 5936-5945.
47. W. Li, P. B. Arockiam, C. Fischmeister, C. Bruneau and P. H. Dixneuf, *Green Chem.*, 2011, **13**, 2315-2319.
48. L. Ackermann, A. Althammer and R. Born, *Tetrahedron*, 2008, **64**, 6115-6124.
49. L. Ackermann, A. Althammer and R. Born, *Synlett*, 2007, **2007**, 2833-2836.
50. K. Cheng, Y. Zhang, J. Zhao and C. Xie, *Synlett*, 2008, **2008**, 1325-1330.
51. L. Ning and Y. Zhengkun, *Chem. Eur. J.*, 2010, **16**, 787-791.
52. K. Korvorapun, N. Kaplaneris, T. Rogge, S. Warratz, A. C. Stückl and L. Ackermann, *ACS Catal.*, 2018, **8**, 886-892.
53. L. Ackermann, R. Born and P. Álvarez-Bercedo, *Angew. Chem. Int. Ed.*, 2007, **46**, 6364-6367.
54. E. Ramos-Cordoba, V. Postils and P. Salvador, *J. Chem. Theor. Comput.*, 2015, **11**, 1501-1508.
55. G. Skara, M. Gimferrer, F. De Proft, P. Salvador and B. Pinter, *Inorg. Chem.*, 2016, **55**, 2185-2199.
56. Gaussian 09, Revision E.01. M. J. Frisch, G. W. Trucks, H. B. Schlegel, G. E. Scuseria, M. A. Robb, J. R. Cheeseman, G. Scalmani, V. Barone, G. A. Petersson, H. Nakatsuji, X. Li, M. Caricato, A. V. Marenich, J. Bloino, B. G. Janesko, R. Gomperts, B. Mennucci, H. P. Hratchian, J. V. Ortiz, A. F. Izmaylov, L. Sonnenberg, D. Williams-Young, F. Ding, F. Lipparini, F. Egidi, J. Goings, B. Peng, A. Petrone, T. Henderson, D. Ranasinghe, J. Zakrzewski, J. Gao, N. Rega, G. Zheng, W. Liang, M. Hada, M. Ehara, K. Toyota, R. Fukuda, J. Hasegawa, M. Ishida, T. Nakajima, Y. Honda, O. Kitao, H. Nakai, T. Vreven, K. Throssell, J. Montgomery, J. A., J. E. Peralta, F. Ogliaro, M. J. Bearpark, J. J. Heyd, E. N. Brothers, K. N. Kudin, V. N. Staroverov, T. A. Keith, R. Kobayashi, J. Normand, K. Raghavachari, A. P. Rendell, J. C. Burant, S. S. Iyengar, J. Tomasi, M. Cossi, J. M. Millam, M. Klene, C. Adamo, R. Cammi, J. W. Ochterski, R. L. Martin, K. Morokuma, O. Farkas, J. B. Foresman and D. J. Fox, Gaussian Inc., Wallingford CT, 2009.
57. B. Li, T. Roisnel, C. Darcel and P. H. Dixneuf, *Dalton Trans.*, 2012, **41**, 10934-10937.
58. A. S. Bhanu Prasad, T. M. Stevenson, J. R. Citineni, V. Nyzam and P. Knochel, *Tetrahedron*, 1997, **53**, 7237-7254.
59. M. C. Hansen and S. L. Buchwald, *Org. Lett.*, 2000, **2**, 713-715.
60. J. J. Mousseau, F. Vallée, M. M. Lorion and A. B. Charette, *J. Am. Chem. Soc.*, 2010, **132**, 14412-14414.
61. S. Oi, Y. Ogino, S. Fukita and Y. Inoue, *Org. Lett.*, 2002, **4**, 1783-1785.

This journal is © The Royal Society of Chemistry 2018

Catal. Sci. Technol., 2018, **00**, 1-3 | **9**